Supporting Information

Permethylation of ribonucleosides provides enhanced mass spectrometry quantification of post-transcriptional RNA modifications

Yixuan Xie[1,2], Kevin A. Janssen[2], Alessandro Scacchetti[3], Elizabeth G. Porter,[1,2] Zongtao Lin,[1] Roberto Bonasio[3], Benjamin A. Garcia[*,1,2]

[1]Department of Biochemistry and Molecular Biophysics, Washington University School of Medicine, St. Louis, Missouri 63110, United States.
[2]Epigenetics Institute, Department of Biochemistry and Biophysics, Perelman School of Medicine, University of Pennsylvania, Philadelphia, Pennsylvania 19104, United States.
[3]Epigenetics Institute, Department of Cell and Developmental Biology, Perelman School of Medicine, University of Pennsylvania, Philadelphia, Pennsylvania 19104, United States.

**Correspondence and requests for materials should be addressed to B.A.G. (email: bagarcia@wustl.edu)*

Table of Contents:

Additional Experimental Procedures

Optimization of Collision Energies. For underivatized ribonucleosides, low collision energy (~10 eV) was utilized for the identification and quantification due to the unstable nature of the ribonucleosides. Because the permethylation can enhance the stability of the precursor ions in the gas phase, the energy required for the fragmentation needed optimization. Therefore, we optimized the collision energies ranging from 10 to 35 eV for the permethylated ribonucleosides to obtain optimal signals of fragment ions. As shown in **Figure S7**, responses of most permethylated ribonucleosides first increased with rising collision energy caused by more efficient fragmentation of the precursor ions. Signal decreased when the collision energy was set greater than 20 eV, potentially due to over-fragmentation under the high collision energy. As a result, 15-20 eV yielded optimal signals for most permethylated ribonucleosides.

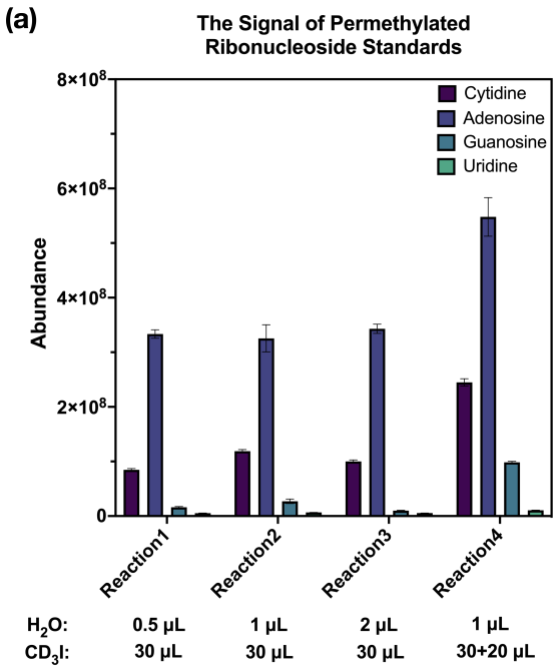

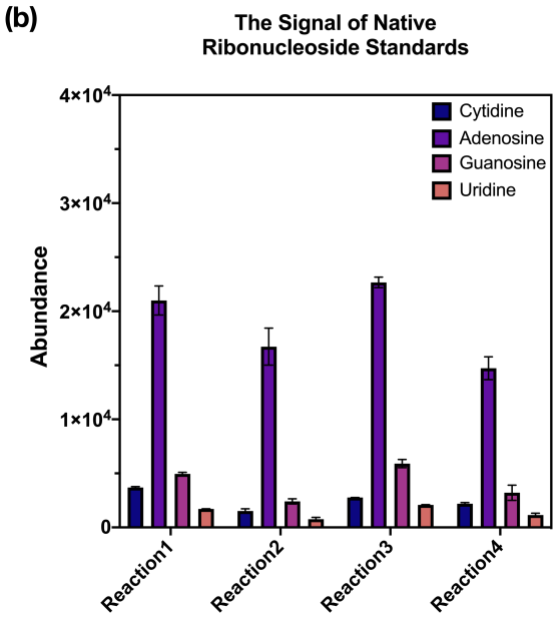

Figure S1. Optimization of the permethylation reaction. The reaction was monitored by the signal of (**a**) permethylated ribonucleosides, and (**b**) unreacted ribonucleosides.

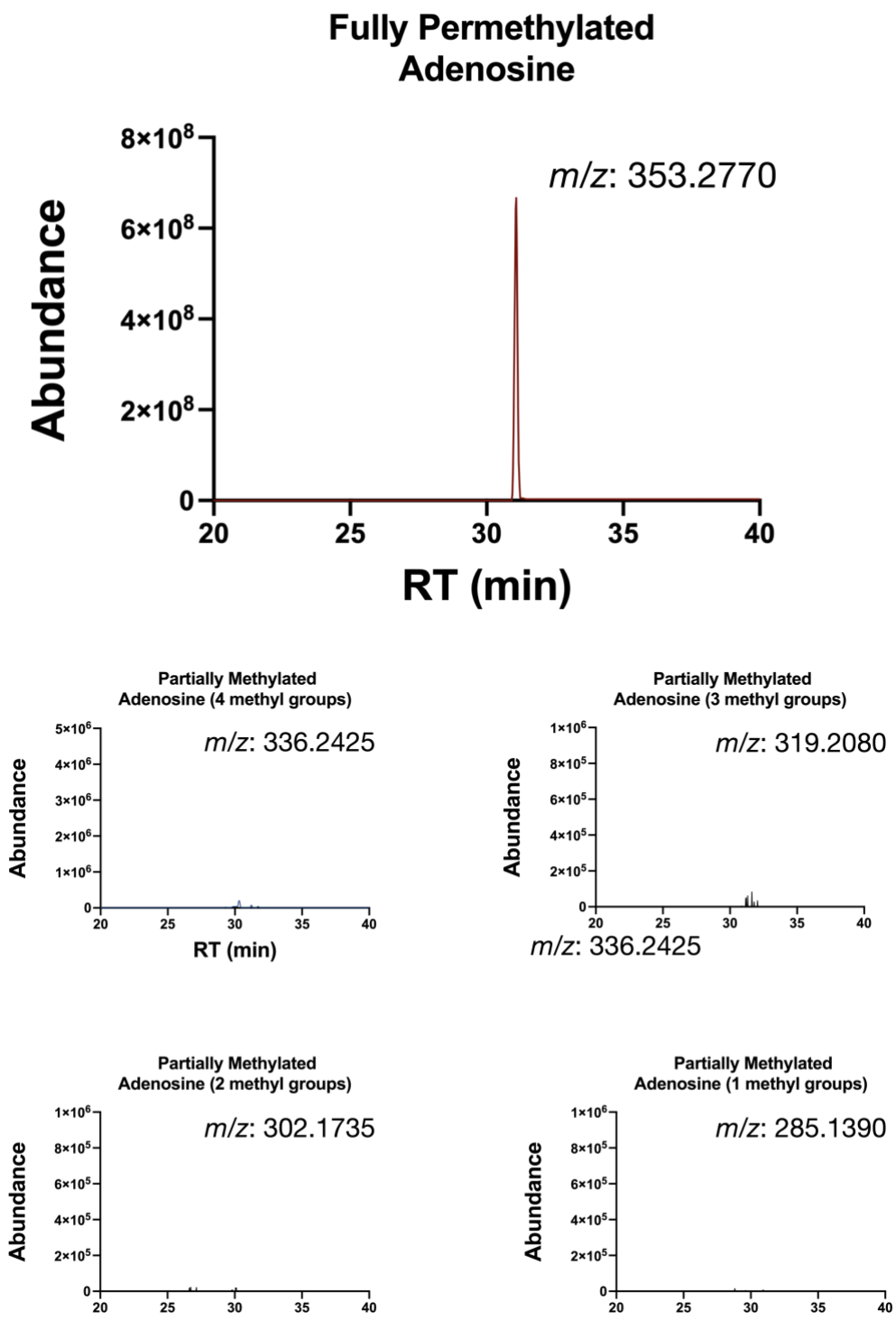

Figure S2. LC-MS chromatography of permethylated and partially methylated adenosines. Fully permethylated adenosine was monitored at *m/z* 353.2770, and four different partially methylated adenosines (with different methylation degrees) were monitored at *m/z* 336.2425, 319.2080, 302.1735, 285.1390, respectively.

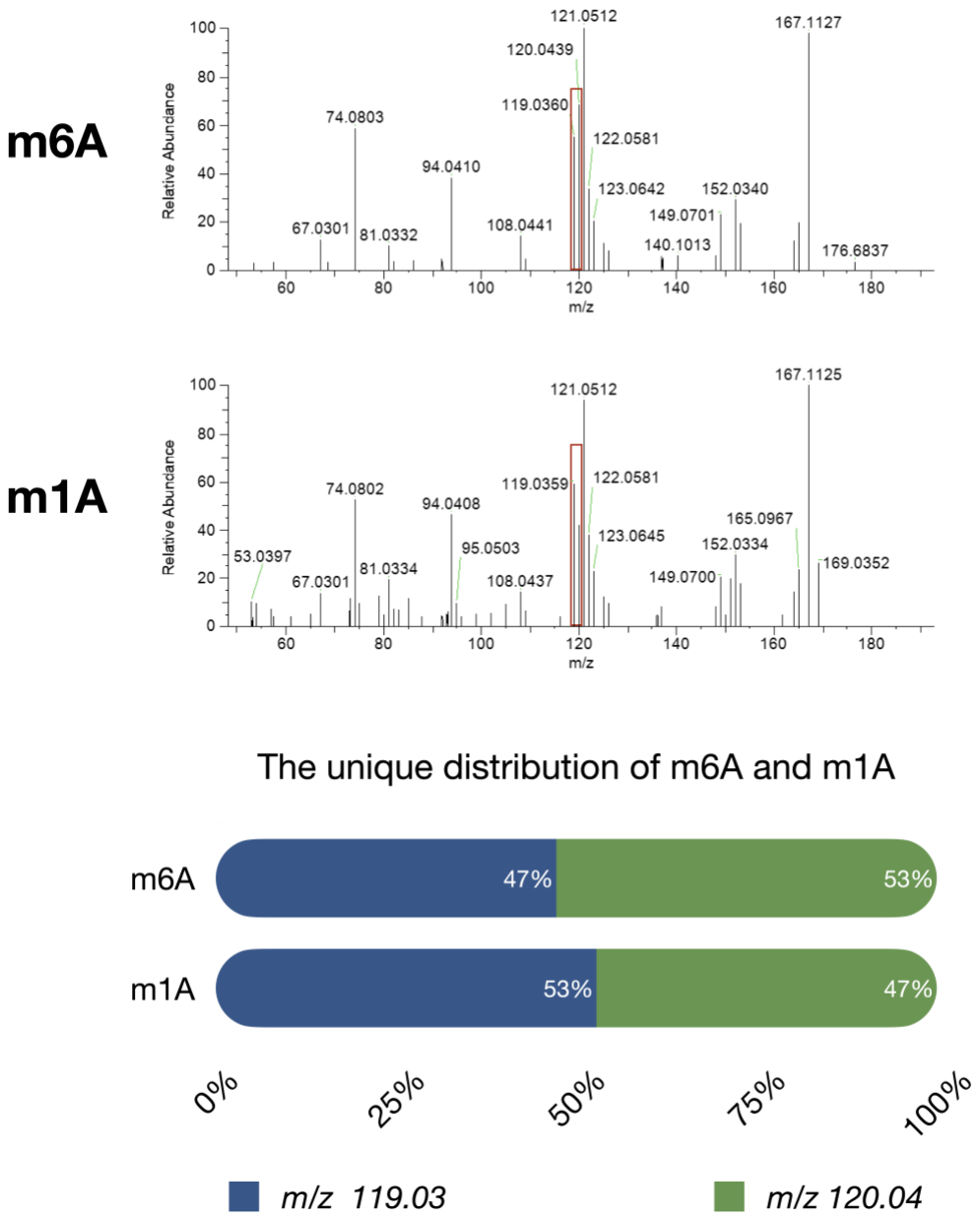

Figure S3. Differentiation of m^6A and m^1A using MS3. The fragmentation from the nucleotide base, *m/z* 167.11, was selected for further fragmentation. The unique pattern at *m/z* 119.03 and *m/z* 120.04 could be used to distinguish m^6A and m^1A.

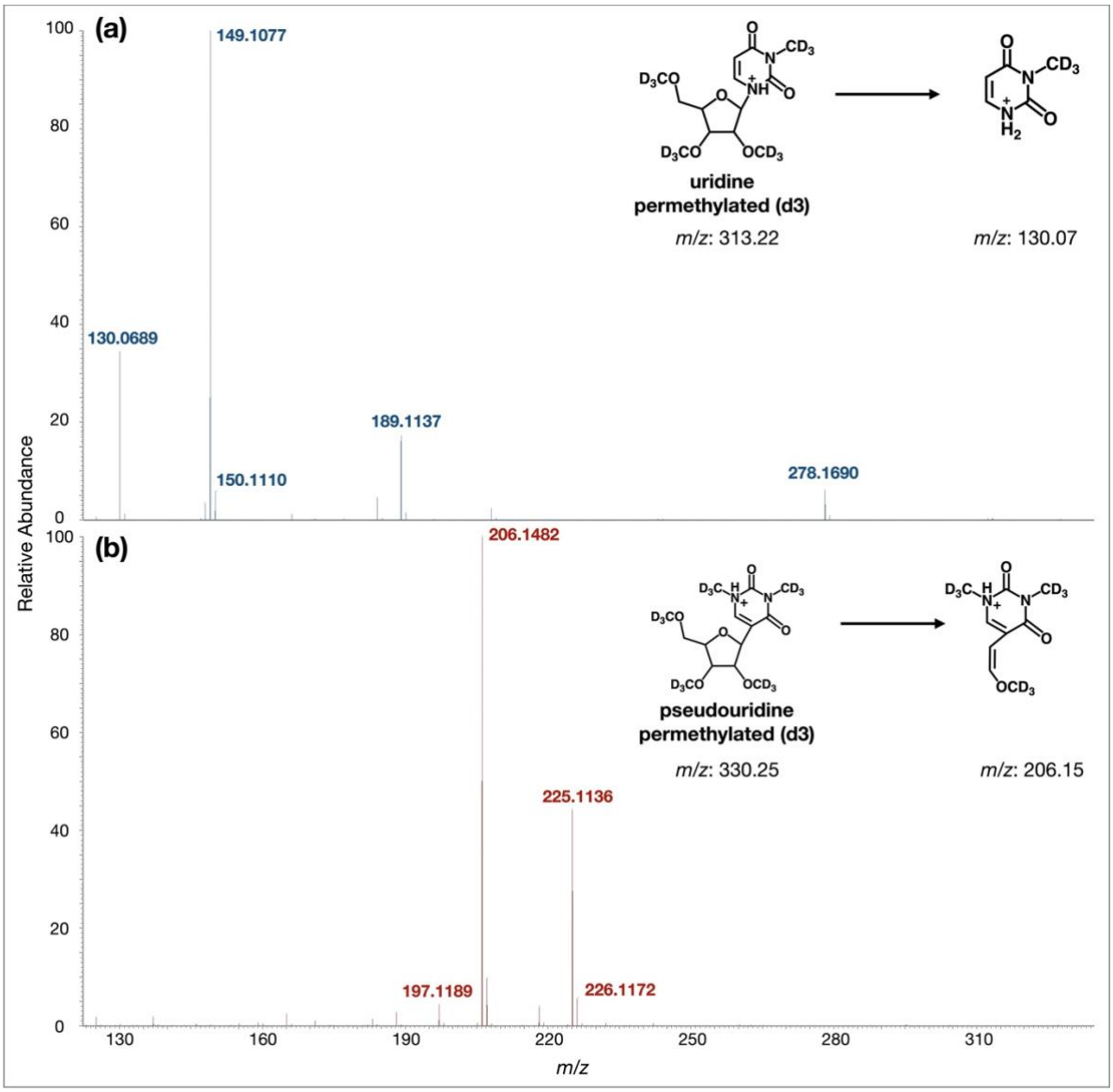

Figure S4. LC-MS/MS spectra of two permethylated isomers: uridine (U) and pseudouridine (Ψ). MS/MS spectra of the methylated(d_3)-labeled protonated precursor ions at (**a**) *m/z* 313.22 for U and (**b**) *m/z* 330.25 for pseudouridine Ψ. HCD Fragmentation of U resulted in signals at m/z 149.11 and m/z 130.07 as the two most abundant fragment ions, while the fragmentation of Ψ produced signals at m/z 206.15 and m/z 22.5.11 as the two most abundant fragment ions.

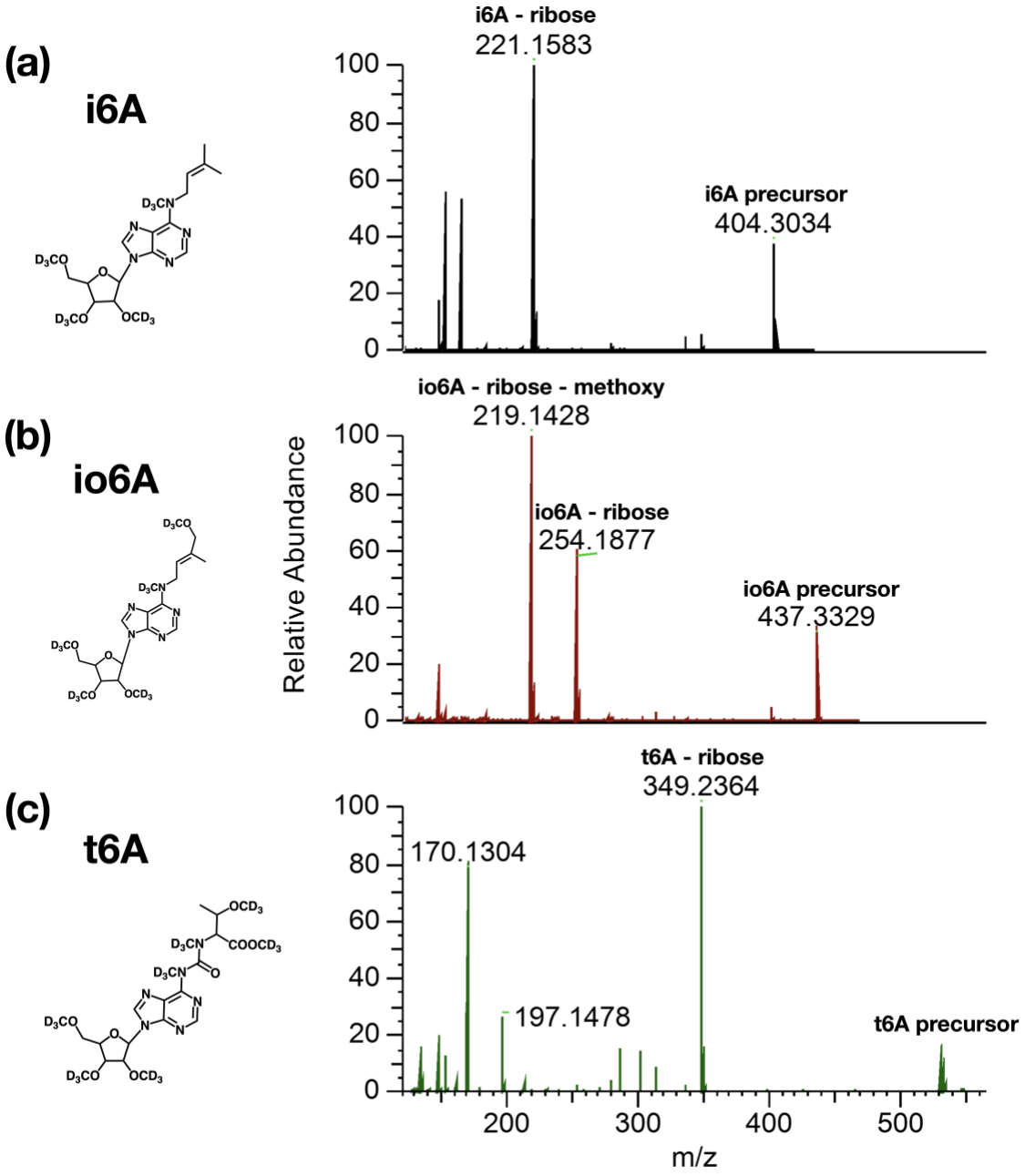

Figure S5. Tandem MS/MS spectra of adenosine modifications. The methylated(d_3)-labeled (**a**) i^{6}A, (**b**) io^{6}A, and (**c**) t^{6}A yielded their signature fragmentation patterns.

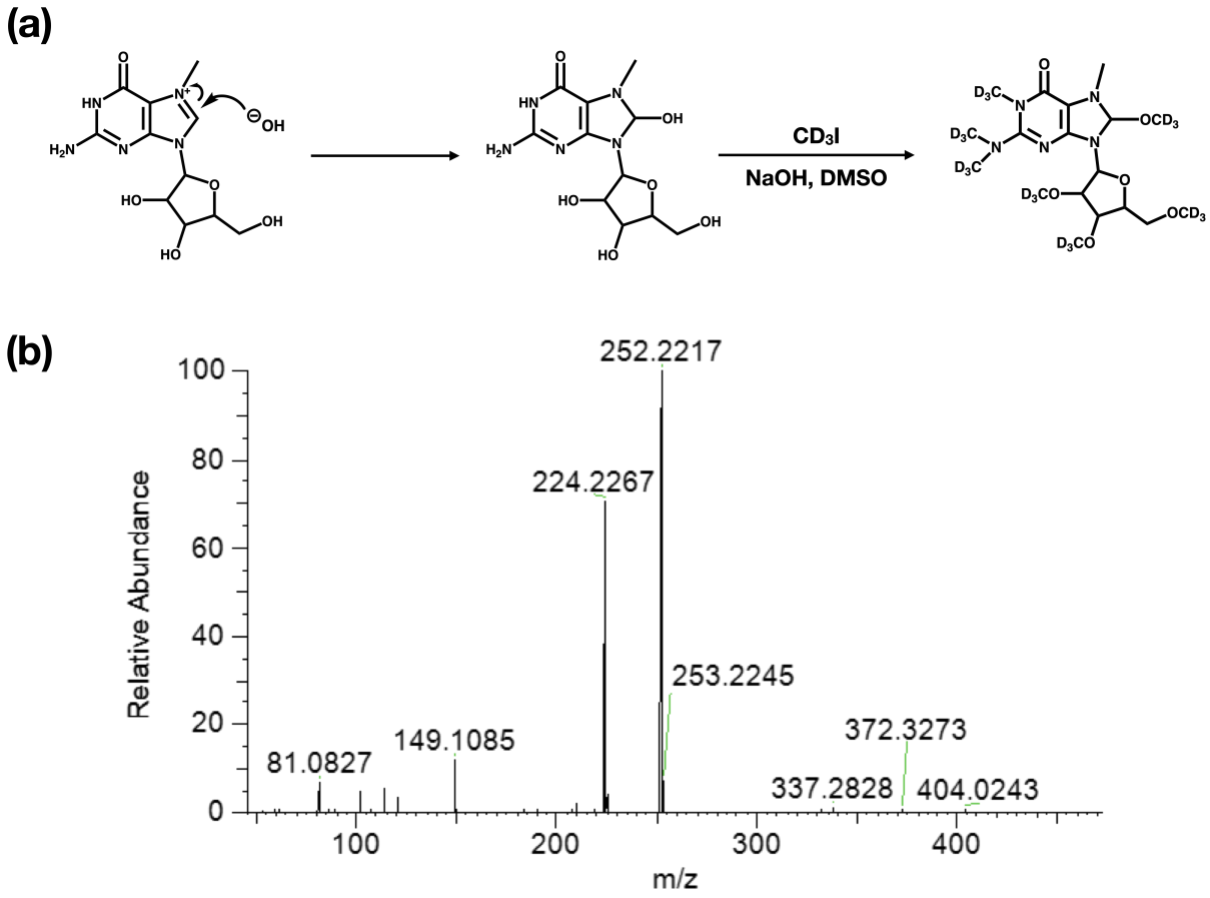

Figure S6. Permethylation reaction of m^7G (7-methylguanosine). (a) Due to m^7G being positively charged, an extra hydroxyl group was added. (**b**) The fragment at *m/z* 252.2217 was detected by monitoring the precursor ion of permethylated m^7G at *m/z* 435.3671.

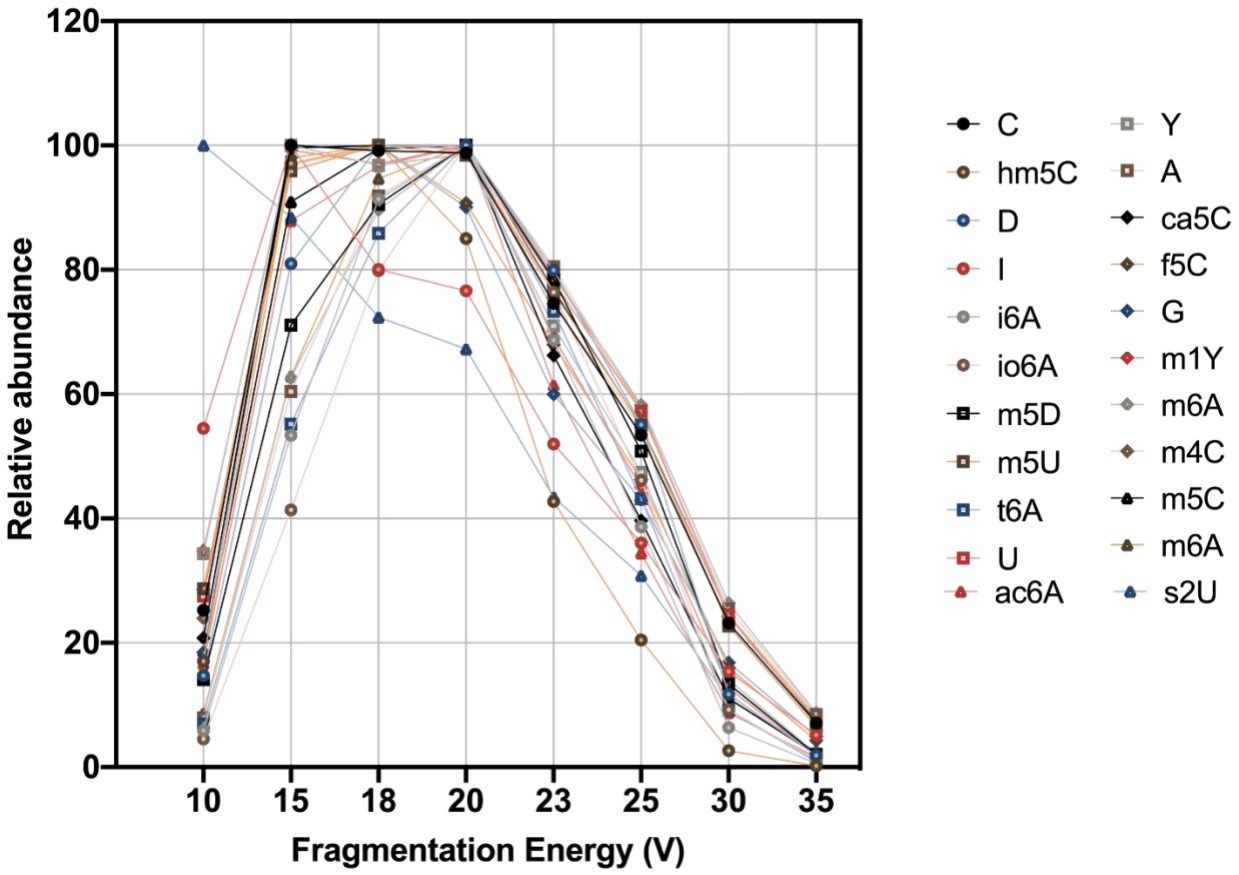

Figure S7. Optimization of collision energy. Permethylated ribonucleoside standards were fragmented under collision energies ranging from 10 to 35 eV to obtain the optimal signal for MS analysis.

Table S1. The dynamic MRM transitions for monitoring ribonucleosides.

No.	Compound Full Name	Common Name	Start Time (min)	End Time (min)	Precursor Ion (*m/z*)	Product Ion (*m/z*)	Collision Energy (V)
1	5-formylcytidine	f^5C	1.5	2.3	357.26	174.11	18
2	5-formyl-2'-*O*-methylcytidine	f^5Cm	1.5	2.3	354.24	174.11	18
3	cytidine	C	2.2	2.8	329.27	146.12	15
4	2'-*O*-methylcytidine	Cm	2.2	2.8	326.25	146.12	15
5	N^4,N^4-dimethylcytidine	$m^{4,4}C$	2.2	2.8	323.23	140.08	15
6	N^4,N^4,2'-*O*-trimethylcytidine	$m^{4,4}Cm$	2.2	2.8	320.21	140.08	15
7	N^4-methylcytidine*	m^4C	2.2	2.8	326.25	143.1	15
8	3-methylcytidine*	m^3C	2.2	2.8	326.25	143.1	15
9	N^4,2'-*O*-dimethylcytidine*	m^4Cm	2.2	2.8	323.23	143.1	15
10	3-methyl-2'-*O*-methylcytidine*	m^3Cm	2.2	2.8	323.23	143.1	15
11	5-carboxylcytidine	ca^5C	2.54	3.14	390.29	207.14	18
12	5-carboxyl-2'-*O*-methylcytidine	ca^5Cm	2.54	3.14	387.28	207.14	18
13	inosine	I	3.3	3.9	337.23	154.08	15
14	2'-*O*-methylinosine	Im	3.3	3.9	334.21	154.08	15
15	1-methylinosine	m^1I	3.3	3.9	334.21	151.06	15
16	1,2'-*O*-dimethylinosine	m^1Im	3.3	3.9	331.19	151.06	15
17	5-methylcytidine	m^5C	3.35	3.95	343.25	160.14	15
18	5,2'-*O*-dimethylcytidine	m^5Cm	3.35	3.95	340.26	160.14	15
19	N^4-acetylcytidine	ac^4C	3.35	4.15	354.24	171.1	15
20	N^4-acetyl-2'-*O*-methylcytidine	ac^4Cm	3.35	4.15	351.22	171.1	15
21	2-thiocytidine	s^2C	3.4	4	345.24	162.1	15
22	dihydrouridine	D	3.6	4.4	315.23	191.13	20
23	1-methylpseudouridine*	m^1Y	4.3	4.9	327.23	203.13	18
24	3-methylpseudouridine*	m^3Y	4.3	4.9	327.23	203.13	18
25	pseudouridine	Y	4.3	4.9	330.25	206.15	18
26	2'-*O*-methylpseudouridine	Ym	4.3	4.9	327.23	206.15	18
27	5-hydroxymethylcytidine	hm^5C	4.6	5.3	376.31	193.16	18
28	2'-*O*-Methyl-5-hydroxymethylcytidine	hm^5Cm	4.6	5.3	373.29	193.16	18
29	N^6-acetyladenosine	ac^6A	4.9	5.5	378.25	195.11	20
30	3-methyluridine	m^3U	5.2	5.8	310.2	127.05	18
31	3,2'-*O*-dimethyluridine	m^3Um	5.2	5.8	307.18	127.05	18
32	2-thiouridine	s^2U	5.2	5.8	329.19	146.05	10
33	2-thio-2'-*O*-methyluridine	s^2Um	5.2	5.8	326.17	146.05	10
34	uridine	U	5.2	5.8	313.22	130.07	18
35	2'-*O*-methyluridine	Um	5.2	5.8	310.2	130.07	18
36	adenosine	A	5.4	6	353.28	170.13	20
37	2'-*O*-methyladenosine	Am	5.4	6	350.26	170.13	20

38	2,8-dimethyladenosine	$m^{2,8}A$	5.4	6	381.31	198.16	20
39	2-methyladenosine*	$m^{2}A$	5.4	6	367.29	184.15	20
40	8-methyladenosine*	$m^{8}A$	5.4	6	367.29	184.15	20
41	*N*^{6},*N*^{6}-dimethyladenosine	$m^{6,6}A$	5.6	6	347.24	164.09	20
42	*N*^{6},*N*^{6},2'-*O*-trimethyladenosine	$m^{6,6}Am$	5.6	6	344.22	164.09	20
43	*N*^{6}-methyladenosine*	$m^{6}A$	5.6	6	350.26	167.11	20
44	*N*^{6},2'-*O*-dimethyladenosine*	$m^{6}Am$	5.6	6	347.24	167.11	20
45	1-methyladenosine*	$m^{1}A$	5.6	6	350.26	167.11	20
46	1,2'-*O*-dimethyladenosine*	$m^{1}Am$	5.6	6	347.24	167.11	20
47	5-hydroxyuridine	$ho^{5}U$	5.85	6.45	346.24	163.1	18
48	5-methyldihydrouridine	$m^{5}D$	5.85	6.65	329.25	205.15	20
49	5-hydroxycytidine	$ho^{5}C$	6	6.6	362.3	179.15	15
50	guanosine	G	7.05	7.65	386.31	203.16	18
51	2'-*O*-methylguanosine	Gm	7.05	7.65	383.29	203.16	18
52	1-methylguanosine*	$m^{1}G$	7.05	7.65	383.29	200.14	18
53	2-methylguanosine*	$m^{2}G$	7.05	7.65	383.29	200.14	18
54	1,2'-*O*-dimethylguanosine*	$m^{1}Gm$	7.05	7.65	380.27	200.14	18
55	2,2'-*O*-dimethylguanosine*	$m^{2}Gm$	7.05	7.65	380.27	200.14	18
56	*N*^{2},*N*^{2}-dimethylguanosine	$m^{2,2}G$	7.05	7.65	380.27	197.12	18
57	*N*^{2},*N*^{2},2'-*O*-trimethylguanosine	$m^{2,2}Gm$	7.05	7.65	377.27	197.12	18
58	5-carbamoylmethyluridine	$ncm^{5}U$	7.2	7.8	404.23	221.09	18
59	5-carbamoylmethyl-2'-*O*-methyluridine	$ncm^{5}Um$	7.2	7.8	401.29	221.16	18
60	5-methyluridine	$m^{5}U$	7.35	7.95	327.23	144.09	18
61	5,2'-*O*-dimethyluridine	$m^{5}Um$	7.35	7.95	324.21	144.09	18
62	*N*^{2},*N*^{2},7-trimethylguanosine	$m^{2,2,7}G$	7.4	8	429.33	246.18	25
63	*N*^{2},7-dimethylguanosine	$m^{2,7}G$	7.4	8	432.35	249.20	25
64	*N*^{2},7,2'-*O*-trimethylguanosine	$m^{2,7}Gm$	7.4	8	429.33	249.20	25
65	7-methylguanosine	$m^{7}G$	7.4	8	435.37	252.22	25
66	*N*^{6}-hydroxymethyladenosine	$hm^{6}A$	7.45	8.05	383.29	200.14	20
67	5-methoxycarbonylmethyluridine	$mcm^{5}U$	9.45	10.15	405.29	159.1	18
68	5-methoxycarbonylmethyl-2'-*O*-methyluridine	$mcm^{5}Um$	9.5	10.1	402.28	159.1	18
69	*N*^{6}-(cis-hydroxyisopentenyl)adenosine	$io^{6}A$	11.05	11.55	437.33	254.19	20
70	*N*^{6}-methyl-*N*^{6}-threonylcarbamoyladenosine	$m^{6}t^{6}A$	11.15	11.65	529.37	346.23	20
71	*N*^{6}-threonylcarbamoyladenosine	$t^{6}A$	11.15	11.65	532.38	349.24	20
72	*N*^{6}-isopentenyladenosine	$i^{6}A$	12.6	13.1	404.31	221.16	20
73	8-hydroxyguanosine	$ho^{8}G$	12.75	13.35	419.34	236.19	18

* The corresponding compounds have the same transition, and the methyl position can be differentiated with MS^n fragmentation.

Table S2. Summary of the number of theoretical plates for underivatized and permethylated ribonucleoside analyses.

Ribonucleoside	Retention time (min)	Peak Width (min)	Plate number (N)
C	1.22	0.08	3721
U	1.71	0.1	4679
A	2.56	0.15	4660
G	2.71	0.16	4590
C (permethylated)	2.51	0.1	10080
U (permethylated)	5.38	0.16	18090
A (permethylated)	5.67	0.18	15876
G (permethylated)	7.3	0.18	26316

Table S3. Summary of linearities of permethylated ribonucleoside standards.

Ribonucleoside	[Mass+H]	Calibration Curve	Linear Range (μg/mL)	LOD (fmol)	LOQ (fmol)	Linear Regression Coefficients (R^2)	CV (%)
A	353.28	Y = 434596*X + 995861	0.0001-0.2	0.028	0.094	0.998	5.70
G	386.31	Y = 154199*X + 402855	0.0001-0.2	0.026	0.086	0.998	2.09
C	329.27	Y = 413520*X - 89569	0.001-0.2	0.030	0.101	0.998	6.51
m^5C	343.25	Y = 1317655*X + 7545963	0.001-0.2	0.029	0.097	0.998	3.11
U	313.22	Y = 6470*X + 17004	0.001-0.5	0.319	1.064	0.998	4.82
m^5U	327.23	Y = 24213*X + 346904	0.001-0.5	0.306	1.019	0.996	4.39
D	315.23	Y = 55.33*X + 457.3	0.02-0.5	6.344	21.149	0.998	6.18
m^5D	329.25	Y = 1161*X + 22377	0.02-0.5	6.074	20.248	0.995	3.02
I	337.23	Y = 32018*X + 96970	0.0001-0.2	0.030	0.099	0.992	3.56
Y	330.25	Y = 19897*X + 120645	0.0001-0.5	0.303	1.009	0.998	4.29
hm^5C	376.31	Y = 2533470*X + 21278753	0.0001-0.2	0.027	0.089	0.994	3.16
s^2U	329.19	Y = 5733*X + 4050	0.001-0.2	0.304	0.113	0.996	4.05
io^6A	437.33	Y = 195785*X + 619394	0.00001-0.2	0.023	0.076	0.995	3.36
t^6A	532.38	Y = 3490*X + 40604	0.0001-1	0.019	0.063	0.995	7.37
i^6A	404.31	Y = 371114*X + 2088335	0.0001-0.2	0.025	0.082	0.992	1.92
f^5C	357.26	Y = 49678*X - 1638376	0.001-1	1.3995	4.665	0.994	4.56